PERGAMON

Electrochimica Acta 45 (2000) 4673–4682

ELECTROCHIMICA Acta

www.elsevier.nl/locate/electacta

Formation and corrosion of InP/In contacts in hydrochloric acid

Achim Walter Hassel *, Matsuhide Aihara, Masahiro Seo

Laboratory of Interfacial Electrochemistry, Graduate School of Engineering, Hokkaido University, Sapporo, Japan

Received 27 December 1999

Abstract

Flatband potentials, charge carrier concentrations and their frequency dispersions of p-type and n-type InP in 1.0 M HCl were determined. The cathodic decomposition of InP in this acidic solution is compared with the deposition process of indium from 1.0 M-HCl containing 0.1 M $InCl_3$. The share of the involved reactions, hydrogen evolution, InP decomposition and indium deposition are investigated. The reaction rates are generally smaller on p-type InP and the reaction speed is much slower but the principal reactions are the same. The kinetics of the indium deposition and dissolution are studied in detail. These reactions are discussed in terms of the preparation of watersplitting photoelectrodes with modified surfaces. © 2000 Elsevier Science Ltd. All rights reserved.

Keywords: Indium phosphide; Semiconductor corrosion; Indium deposition; Schottky barrier; Watersplitting photoelectrode

1. Introduction

InP is a promising material for high-speed-transistors (>1 GHz), optoelectronic devices and watersplitting photoelectrodes [1–3]. The main advantages are the favourable band gap and position of the Fermi level, the high charge carrier mobility and the generally high corrosion resistance. However, under special conditions such as high overpotentials, aggressive electrolytes or illumination, the corrosion or photocorrosion can increase significantly [4–7]. Beside the unintentional loss of material, this offers the chance for a modification of the material. Examples are the surface modification by metal deposition [7–9] and the formation of porous InP by anodic oxidation in HCl which has been demonstrated recently in analogy to the preparation of porous silicon [10,11].

InP forms Schottky barriers with many metals [12,13]. The barrier heights are generally small. Attempts were made to modify an InP surface by covering it with small metallic indium bumps. This should increase the efficiency of hydrogen evolution if this system is used as a watersplitting photoelectrode. The success of this method was very limited due to the high overpotential for hydrogen evolution at metallic indium [14]. If other metals are used directly on the InP interface, the barrier remains small for reactive metals such as aluminium, nickel or iron, or it increases significantly for the less reactive metals such as gold, copper or silver [15–17]. The first group of metals is not very promising either due to their corrosion tendency or due to their charge transfer blockage, resulting from their passivation at the electrolyte interface. For the latter group, on the other hand, the charge transfer is hindered at the higher Schottky barrier.

A consequent idea would be now to use a more complex system which combines the advantages of both metals. InP should be used as the light converting semiconductor, which carries small platinum covered indium bumps. The InP/In interface with its low barrier height would allow an easy charge transfer into the

* Corresponding author. Present address: Max-Planck-Institut für Eisenforschung GmbH, Abteilung für Grenzflächenchemie und Oberflächentechnik, Postfach 140 444, 40074 Düsseldorf, Germany.

E-mail address: hassel@elchem.de (A.W. Hassel).

PII: S0013-4686(00)00619-8

metal and the influence of the In/Pt interface is probably negligible. The influence of indium interlayers in InP/noble metal contacts has already been studied [13]. This sandwich type material has a high potential for material engineering since the position of the Fermi level pinning, and hence, the height of the Schottky barrier can be influenced by a selected metal [13]. Finally the outermost metal layer could be optimised to minimise the kinetic hindrance of the hydrogen evolution reaction.

In this work, the basic reactions of InP or InP/In in hydrochloric acid are investigated. The properties of the blank semiconductor and of completely covered InP are described. The influence of the Schottky barrier at the semiconductor/metal interface is revealed for n-type and p-type electrodes. In/InP contacts are either prepared by cathodic decomposition or by cathodic deposition from $InCl_3$ containing electrolyte.

2. Experimental

The electrochemical cell consisted of a double walled glass vessel with six connectors for electrodes and inlets (gas and electrolyte). The cell was thermostatted to 298 K and kept in complete dark for all experiments. A gold electrode ($A = 4$ cm^2) was used as counter electrode and a silver/silver chloride electrode with salt-bridge acted as reference electrode.

Solutions (1.0 M HCl) were prepared from reagent grade chemicals and ultrapure water (Millipore Q). Comparative studies were performed in 1.0 M HCl solutions containing 0.1 M $InCl_3$. They were deaerated with ultrapure argon (7.0 N) prior to use. InP single crystals (100) were purchased from Japan Energy, Tokyo. The n-type InP was doped with S, resulting in a bulk charge carrier concentration $N_{D,Bulk} = 3.7 \times 10^{18}$ cm^{-3}and a specific resistance of $R_{Spec} = 1.1 \times 10^{-3}$ Ω cm. The Ohmic back contact was prepared by successive evaporation of Ge (20 nm), Au (80 nm) and Ni (20 nm). The p-type InP was Zn doped with $N_{A,Bulk} = 3.7 \times 10^{18}$ cm^{-3} and $R_{Spec} = 2.6 \times 10^{-2}$ Ω cm. Two successive layers of Zn (20 nm) and Au (80 nm) were used to form the Ohmic back contact. A copper wire was connected to the back side using silver paste and the specimen was embedded into silicone sealant. The specimens were etched in concentrated HCl, washed with ethanol and thoroughly rinsed with water.

All electrochemical measurements were performed using a Solartron Schlumberger frequency response analyser HF 1255B in combination with a Solartron electrochemical interface 1287.

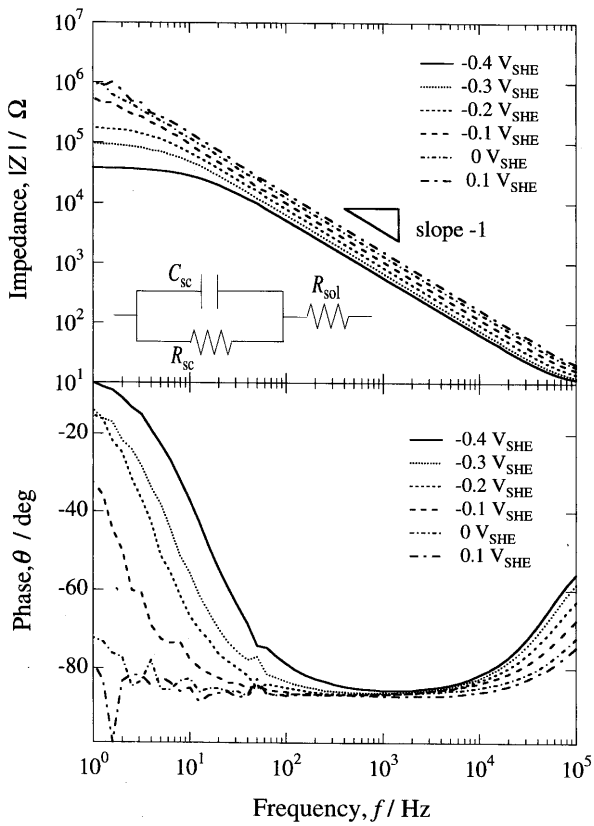

Fig. 1. Impedance spectra of n-InP in 1.0 M HCl. The simple equivalent circuit is given as an insert.

3. Results

3.1. Basic semiconductor properties

The electrochemical behaviour of a semiconductor is determined mainly by the flatband potential E_{FB}, the band gap and the charge carrier concentration N (N_D or N_A) in the space charge layer. Hence, a detailed knowledge of these parameters is indispensable for an understanding of a material's electrochemical behaviour. In order to get a consistent set of these basic parameters, they were determined under these very conditions.

Some representative electrochemical impedance spectra (1 Hz $\leq f \leq$ 100 kHz) of n-InP in 1.0 M HCl are shown in Fig. 1 for various electrode potentials. The spectra prove not only the validity of the simple equivalent circuit which is given as an insert, but demonstrate also the potential dependence of the capacity and the resistance of the semiconductor/electrode interface.

Mott–Schottky plots of these data are shown in Fig. 2 for different frequencies. If the capacity of the space charge layer C_{SC} is plotted as a function of the electrode potential E according to,

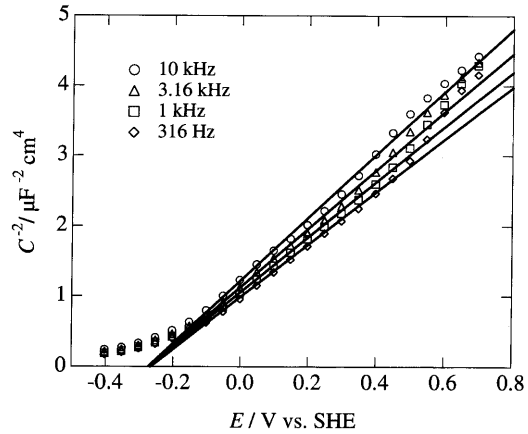

Fig. 2. Mott–Schottky plots of n-InP in 1.0 M HCl for different frequencies.

$$\frac{1}{C_{SC}^2} = \frac{2}{qN\varepsilon_0\varepsilon_r}\left(E - E_{FB} - \frac{kT}{q}\right) \quad (1)$$

where q, elementary charge; k, Boltzmann constant; and T, temperature. The flatband potential can be determined from an extrapolation to $C_{SC}^{-2} = 0$. The charge carrier concentration can be calculated from the slope, since the vacuum permittivity ε_0 and the relative permittivity of the material ε_r (12.3 [8], 12.1 [18]) are known. This analysis was made for different frequencies, to show the influence of the frequency dispersion on the values.

The results of this analysis are shown in Fig. 3. In Fig. 3a, the charge carrier concentration N_D in the space charge layer is plotted as a function of the frequency. At 1 kHz, it has a value of 2.9×10^{18}cm^{-3} and decreases by 8.8% per decade of frequency. The determination of the charge carrier concentration is most reliable for frequencies between 50 Hz and 30 kHz where the space charge capacity dominates the impedance response of the system. For higher frequencies, the electrolyte resistance determines the impedance and in the low frequency region, the parallel resistance limits the impedance. The flatband potential, on the other hand, shows a much less pronounced frequency dependence in Fig. 3b. Again, the values are most reliable in the frequency window between 50 Hz and 30 kHz where the space charge capacitance dominates. The flat band decreases by 5 mV per decade of frequency. At 1 kHz, it has a value of -0.295 V.

The same analysis was made for p-type InP. As already reported, a second time constant is observed in the impedance spectra of this system. This is usually ascribed to the charge transfer resistance in parallel to the Helmholtz capacity at the semiconductor/electrolyte interface. A detailed description is being skipped here, since the main emphasis is put on the determination of the flat band potential and the charge carrier concentration. Hence, the impedance spectra were analysed only in the frequency range where the space charge capacity can be determined. The results taken from the Mott–Schottky analysis are shown in Fig. 4. As indicated in both figures, the space charge capacity is dominating only in a comparatively small frequency range between 30 and 1500 Hz, which means 1.5 decades. Fig. 4a shows the acceptor concentration as a function of the frequency. At 1 kHz, it has a value of 3.7×10^{18} cm^{-3}. The line which is shown in the figure represents the linear regression, calculated over the space charge capacity dominated region C_{SC} and the region R_{SC} where the resistance of the space charge layer is dominant, but still significantly influenced by the space charge capacity. The slope of this line yields the charge carrier concentration which decreases 3.3% per decade of frequency. The frequency dependency is less pronounced than for the n-InP. In Fig. 4b, the flat band potential is

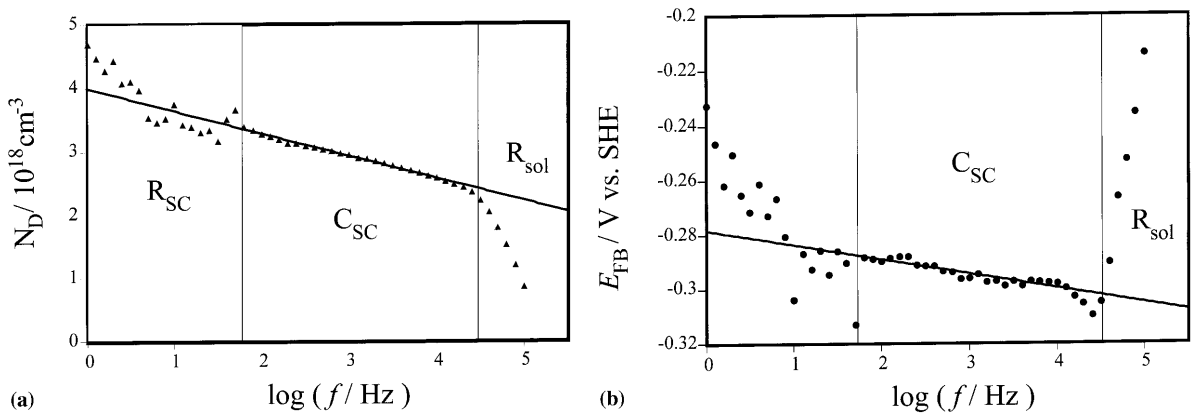

Fig. 3. (a) Frequency dependence of the flat band potential of n-InP in 1.0 M HCl. The regime of any dominating element is indicated in the figure. (b) Frequency dependence of the charge carrier concentration N_D of n-InP in 1.0 M HCl. The regime of any dominating element is indicated in the figure.

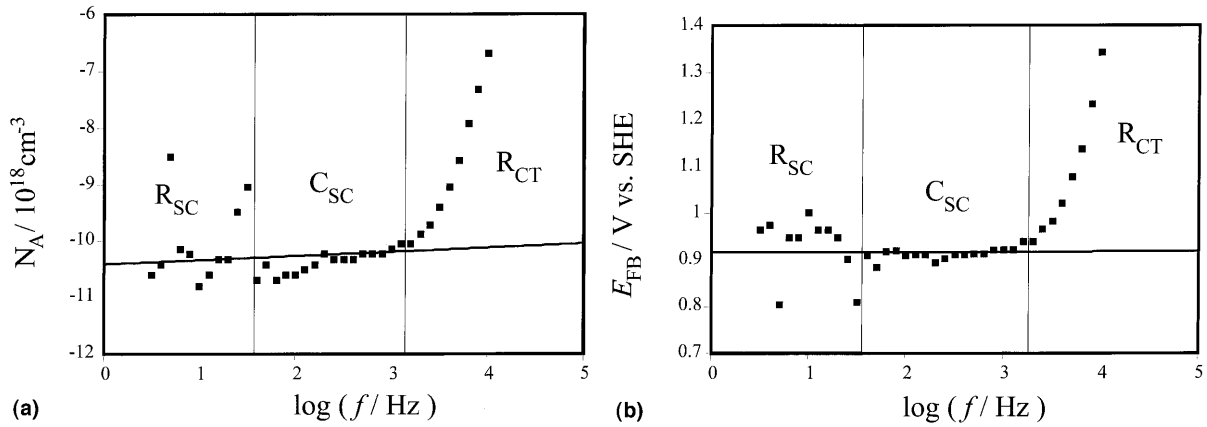

Fig. 4. (a) Frequency dependence of the flat band potential of p-InP in 1.0 M HCl. The regime of any dominating element is indicated in the figure. (b) Frequency dependence of the charge carrier concentration N_A of p-InP in 1.0 M HCl.

plotted as a function of the frequency. Like for the charge carrier concentration, the frequency range where the space charge capacity dominates is limited to a small band of 1.5 decades. A value of 0.92 V is determined at a frequency of 1 kHz. In contrast to n-InP, it is found that flat band potential is almost independent on the frequency. This was also found by Van Wezemael et al. [19] and Uosaki and Kita [1].

3.2. Corrosion of InP in HCl

If InP is polarised cathodically (in dark) in acidic solutions, it decomposes according to

$$InP + 3H^+ + 3e^- \rightarrow In + PH_3\uparrow \quad (2)$$

in parallel to hydrogen evolution

$$2H^+ + 2e^- \rightarrow H_2\uparrow \quad (3)$$

The formation of PH_3 was recently proved by mass spectrometry [20]. The latter reaction will be influenced by the metallic indium which is formed in the first reaction. The kinetic behaviour depends on the amount and morphology of the indium on the semiconductor surface, the type of InP and the amount of hydrogen which was already formed at the electrolyte interface [4,8].

An analysis of the corrosion rate and suggestions on the mechanism become possible, if the metallic indium, formed on the InP surface during cathodic decomposition, is oxidised in a subsequent anodic potential sweep. An example of this procedure is given in Fig. 5. The potentiodynamic anodic polarisation curves (sweep rate, 10 mV s^{-1}) were recorded after polarising the n-type sample potentiostatically at -0.8 V (SHE) for a defined time t_{corr}. The corrosion time was varied in this experiment. The cathodic corrosion charge, as well as the charge of the anodic oxidation peak, were obtained by numerical integration of the corresponding current transients. It is seen that the height increases with increasing corrosion time. The peak shifts to more anodic potentials with increasing corrosion time, or cathodically consumed charge respectively, indicating some kind of kinetic hindrance in the dissolution. As reported before [17], this anodic current peak can be observed on both types of InP. The peak potential was $E_{Peak} = -0.47$ V (SHE) at a sweep rate of 10 mV s^{-1}. It was also shown that the dependence of the peak potential on the cathodic corrosion time t_{corr} or amount of formed indium respectively, was much smaller for n-type InP compared with p-type.

The dissolution reaction,

$$In \rightarrow In^{3+} + 3e^- \quad (4)$$

+ was analysed in more detail with the following experiments. Fig. 6 shows cyclic voltammograms of n-InP in

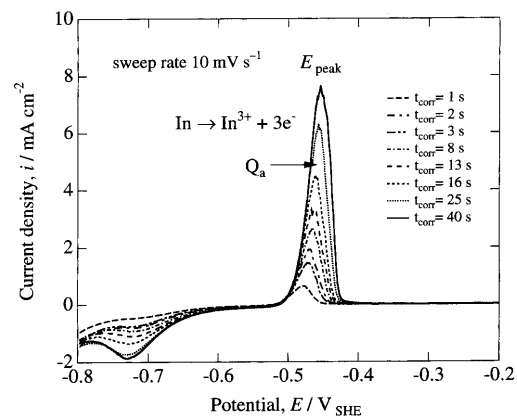

Fig. 5. Potentiodynamic dissolution of indium from n-InP in 1.0 M HCl. The indium was formed potentiostatically at -0.8 V for t_{corr} by cathodic decomposition of the semiconductor.

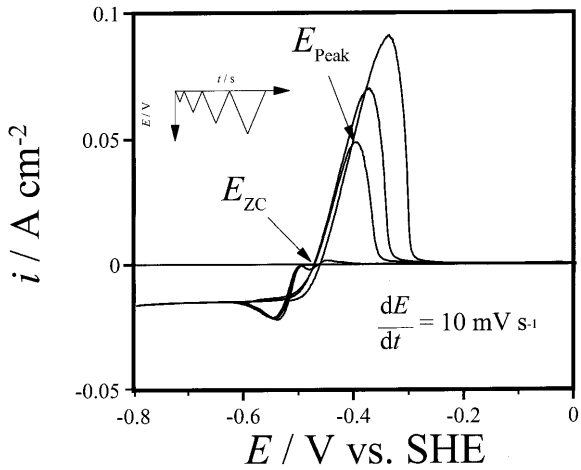

Fig. 6. Cyclic voltammograms of n-InP in 1.0 M HCl containing 0.1 M $InCl_3$. The lower reverse potential was -0.5, -0.6, -0.7 and -0.8 V and the scan rate was $dE/dt = 10$ mV s^{-1}.

1.0 M HCl containing 0.1 M $InCl_3$. The sweeps were started at 0 V and the potential was lowered with a rate of $dE/dt = 10$ mV s^{-1}. After reaching the lower potential limit, the potential was increased immediately with the same rate back to the starting potential of 0 V. For return potentials of -0.1, -0.2, -0.3 and -0.4 V, no significant current flow was observed. With a lower potential limit of -0.5 V, a minor cathodic charge consumption is observed at the very end of the cathodic sweep. Accordingly, a small anodic charge is observed in the subsequent anodic sweep. However, if a more cathodic potential is chosen as the lower limit, the current first increases up to 25 mA cm^{-2} and then drops down to about 20 mA cm^{-2}. Then it remains almost constant for even more cathodic potentials. Neither in the subsequent anodic sweep does the current density changes up to a potential of about -0.5 V. At a potential between -0.5 and -0.4 V the sign of the current changes at the characteristic potential E_{zc}. The term E_{zc} for the potential of zero current is chosen here with respect to the unknown nature of this potential. At higher potentials, an anodic current peak is observed. The potential of maximum current E_{Peak} depends on the lower potential limit or the consumed charge, respectively. It should be noted that the cathodic current density is almost independent on the potential, on the scan direction and shows an excellent reproducibility if the same specimen is cycled many times.

This process was further analysed by the potential time program which is given as an insert in Fig. 7a. The n-type specimen was polarised potentiostatically to -0.8 V for a defined time t_w. The potential was then swept anodically as before. The charge densities which were consumed during potentiostatic cathodic polarisation ($q_{cathodic,potstat}$), during the potential sweep up to E_{zc} ($q_{cathodic,potdyn}$) and above E_{zc} (q_{anodic}) are plotted as a function of the time in Fig. 7a. The amount of deposited In ($q_{cathodic,potstat}$) increases linearly with time, as it is expected for a potential and time independent current. The additionally consumed charge in the first part of the sweep remains constant. Consequently, the charge of the anodic peak increases linearly with a similar slope as the potentiostatic one. The two characteristic potentials E_{zc} and E_{Peak} are analysed in Fig. 7b. The potential of zero current remains unchanged whereas the peak potential shifts to more anodic potentials with increasing amount of deposited indium. This indicates that the dissolution of indium is kinetically hindered.

The same experiments were made with p-type InP. The results are shown in Fig. 8. As for the n-InP $q_{cathodic,potstat}$ increases linearly with time and $q_{cathodic,potdyn}$ remains constant in Fig. 8a. Also for q_{anodic} a linear dependence on the polarisation time is found. Fig. 8b is essentially the same as for the n-InP in Fig. 7b. The main differences are the absolute value of E_{Peak} and its stronger dependence on the waiting time. At this point, it is not clear whether these differences result from a stronger kinetic hindrance. However, one might suggest this from the coincidence of the onset of dissolution E_{zc} for both types of InP.

In Fig. 9, the ratio of anodic and cathodic charge is plotted as a function of the polarisation time or total charge, respectively. Potentiostatic and potentiodynamic cathodic charges were summarised to give the total cathodic charge. Ideally, a value of 1 would indicate a fully reversible deposition/dissolution of indium on the semiconductor surface. This value is found only for n-type InP for polarisation times of 15 s or longer. In the case of p-InP, a significantly smaller value of 0.65 is found in the beginning. For longer polarisation times, however, the ratio tends more and more to unity. This behaviour can be understood easily with the hydrogen evolution reaction (Eq. (3)) in parallel to the indium deposition in the beginning. After complete coverage with indium, the share of this reaction will decrease since the hydrogen evolution has a large overpotential on indium.

Surprisingly, ratios of more than 1 are found for n-InP at shorter polarisation times. Probably a chemical decomposition of the semiconductor leads to a thin layer of species which are oxidised in the following sweep.

In order to analyse the kinetic hindrance of the dissolution process further, the scan rate dependency was investigated. The sample was polarised potentiostatically to -0.8 V for 25 s to deposit a defined amount of indium on the surface. The potential was then switched to E_{zc} and immediately scanned with a scan rate between 3 μV s^{-1} and 300 mV s^{-1}. The peak

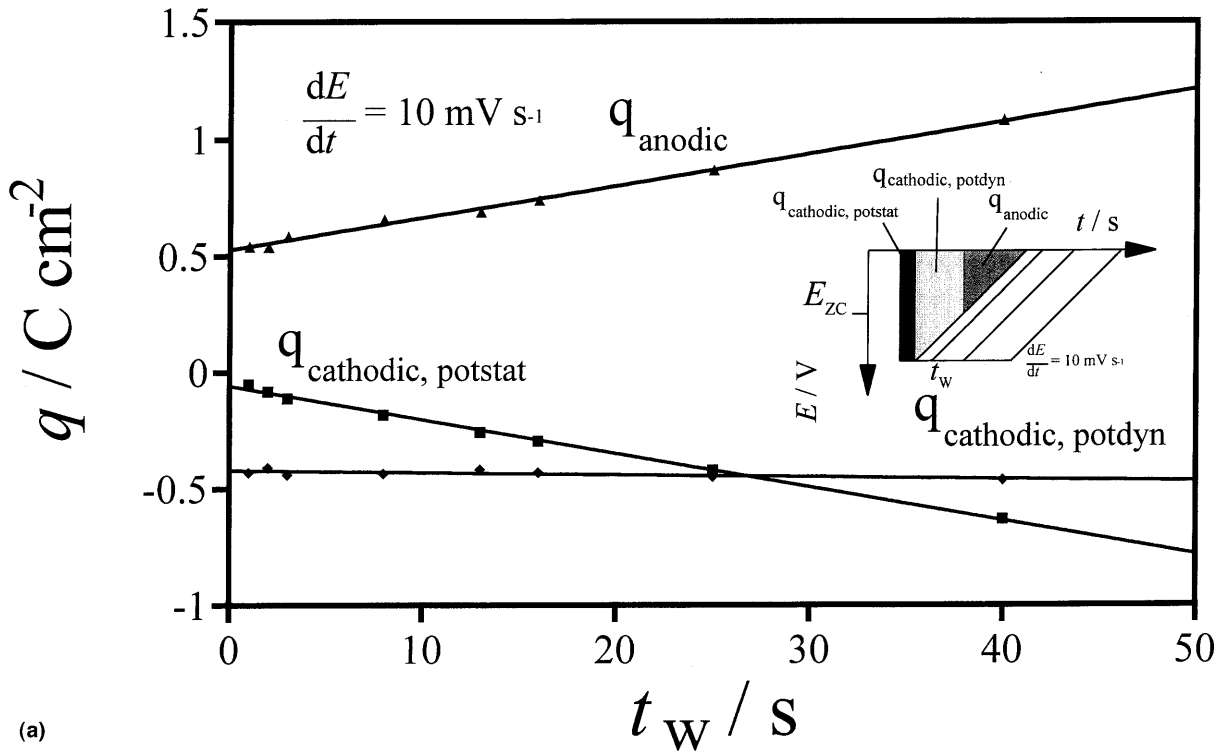

(a)

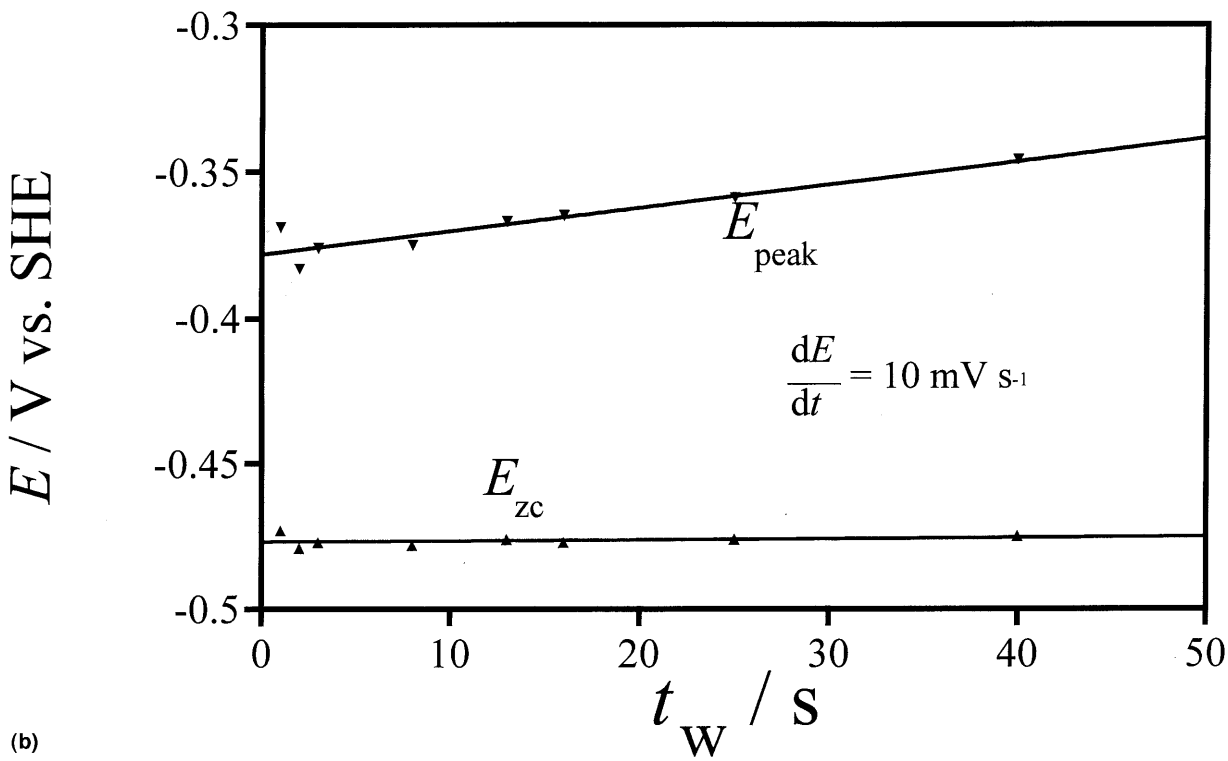

(b)

Fig. 7. (a) Partial charge density as a function of the cathodic polarisation time at −0.8 V of n-InP in 1.0 M HCl containing 0.1 M $InCl_3$. The potential time diagram is given as an insert. Details on the meaning of each charge are given in the text. (b) Potential of the anodic dissolution peak E_{Peak} and potential of zero current E_{zc} as a function of the cathodic polarisation time at −0.8 V of n-InP in 1.0 M HCl containing 0.1 M $InCl_3$. These data were obtained from the same experiments as those in Fig. 7a.

potentials are plotted as a function of the sweep rate in Fig. 10 for both types of InP. A logarithmic scale was chosen with respect to the wide range of scan rates. It is seen, that both types of InP tend to a lower potential limit of −0.45 V. This potential is the equilibrium potential of the InP in this solution. The figure shows

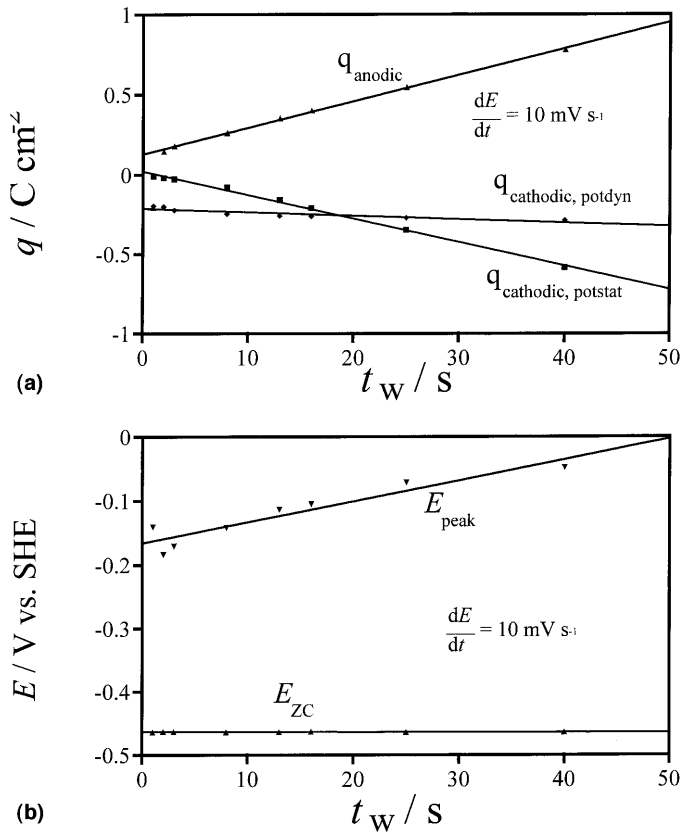

Fig. 8. (a) Partial charge density as a function of the cathodic polarisation time at −0.8 V of p-InP in 1.0 M HCl containing 0.1 M $InCl_3$. The potential time program was the same as shown in the insert in Fig. 7a. Details on the meaning of each charge are given in the text. (b) Potential of the anodic dissolution peak E_{Peak} and potential of zero current E_{zc} as a function of the cathodic polarisation time at −0.8 V of p-InP in 1.0 M HCl containing 0.1 M $InCl_3$. These data were obtained from the same experiments as those in Fig. 8a.

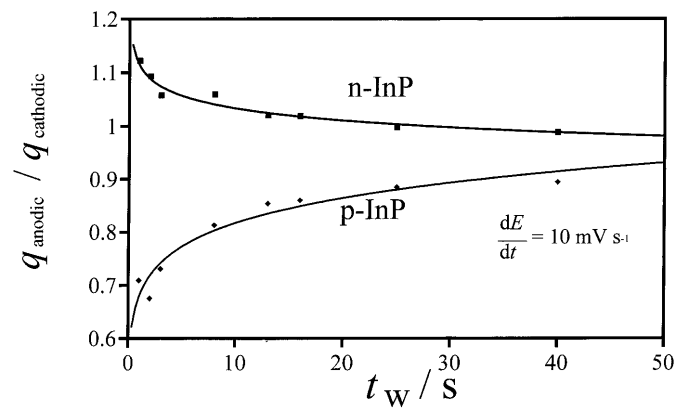

Fig. 9. Ratio between anodic dissolution charge density and cathodic deposition charge density as a function of the cathodic polarisation time t_w at −0.8 V of p-InP in 1.0 M HCl containing 0.1 M $InCl_3$.

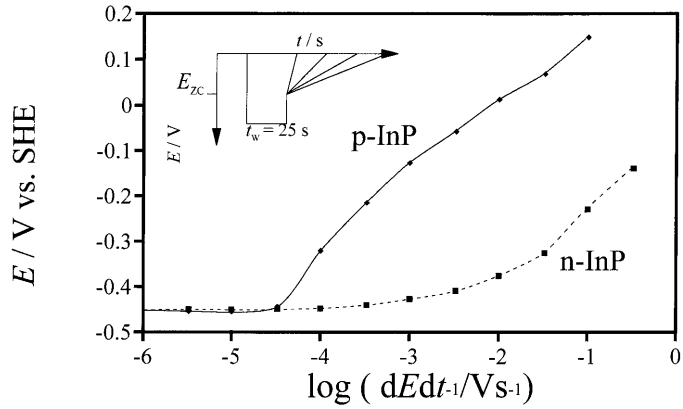

Fig. 10. E_{Peak} as a function of the logarithm of the scan rate for n-type InP and p-type InP in 1.0 M HCl containing 0.1 M $InCl_3$.

clearly that the kinetic hindrance is much stronger for the p-type. With this result, the meaning of the potential of zero current is illuminated. For a moderate sweep rate up to 10 mV s^{-1}, it coincides with the equilibrium potential. For higher sweep rates, it is shifted to more anodic values.

4. Discussion

The results of the experiments described above are summarised in the energy level diagram of Fig. 11. The levels refer on the left side to the vacuum scale and on the right side to the electrochemical scale. The flatband potentials at 1 kHz of both types of InP are plotted, as well as the limiting anodic peak potential which nearly coincides with the E_{zc} at sweep rates up to 10 mV s^{-1}. This potential lays just at the lower edge of the conduction band. The standard normal potentials of the three plausible reactions between In, In^+ and In^{3+} are also given. Significant deviations from these potentials must be expected especially for the decomposition in pure hydrochloric acid, since the concentration of the dissolved In^+ and In^{3+} ions is very low.

For the deposition experiments with $InCl_3$ containing electrolyte on the other hand, the potential is well defined and constant since the concentration in the solution does not change. From a comparison of the potentials, it is concluded that Eq. (4) is the dominant reaction. Surface analytical investigations have shown that a film with significant content of In^+ is formed on InP (111) planes in hydrochloric acid [20]. The fact that the current density in Fig. 6 remains constant for even higher cathodic polarisation proves the absence of In^+ in the deposited film. The tendency to a charge ratio of 1 for both types of InP on the other hand demonstrates that the In is dissolved directly to the trivalent ion. The nature of this reaction can also be proved with an InP electrode with evaporated indium. If this electrode is immersed at a moderate cathodic potential into the $InCl_3$ containing HCl electrolyte and then potentiodynamically scanned to more anodic potentials, the dissolution of indium can be measured. A calculation of the charge proves a dissolution process in agreement with Eq. (4) [21].

A reaction scheme for the decomposition and the dissolution cycle at different stages is given in Fig. 12. On bare InP, decomposition and hydrogen evolution are concurrent reactions in the beginning. With increasing indium coverage, the ratio between both reaction changes since the material transport through the sur-

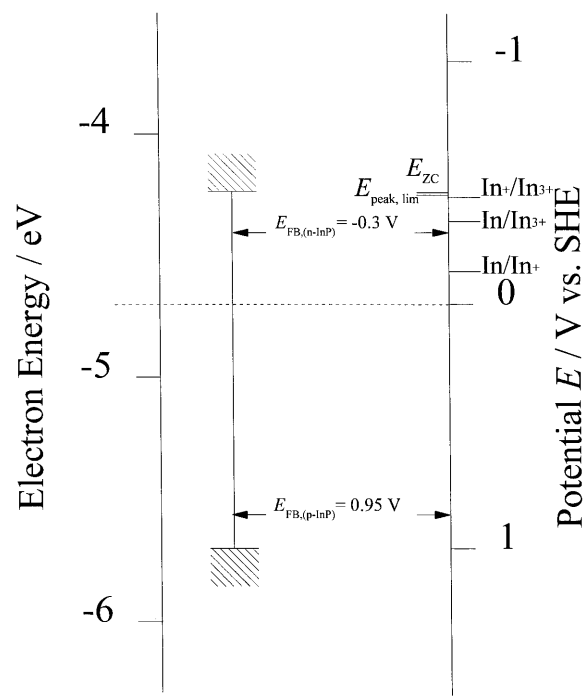

Fig. 11. Energy level diagram of InP.

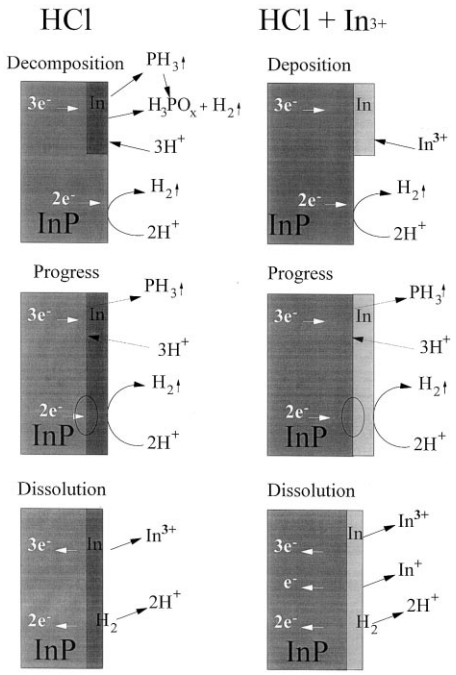

Fig. 12. Schematic of the reactions during decomposition or deposition.

face indium layer is more and more hindered. Therefore, the share of the hydrogen evolution increases for both types of InP [18] with increasing metal coverage. The structure of the indium is expected to be more or less porous since roughly half of the semiconductor is dissolved in the solution. Otherwise, the significant reaction rate even for thicker indium coverages would be hard to explain.

In contrast to the before mentioned, the share of the reactions is quite different for the deposition process. In the very beginning, decomposition, deposition and hydrogen evolution are concurrent reactions. But with the first monolayer of indium, the reaction fraction changes dramatically. While decomposition and hydrogen evolution are slowing down immediately, due to the hindered material transport, or the overpotential of the hydrogen evolution on indium, the indium deposition is not significantly influenced by the thickness of the indium layer. The film should be much more dense compared with the film formed by decomposition. The indium deposition, on the other hand, can proceed continuously at the same rate. The hydrogen evolution is not only important as a concurrent reaction but also influences the total reaction speed. The Schottky barrier at the semiconductor/metal interface can be influenced strongly by electrochemically formed hydrogen. The height of this barrier can be determined either from the reverse saturation current density or from Mott–Schottky plots for solid-state InP-metal contacts. The barrier heights are found to be much smaller (0.4 eV) for n-InP-In than for p-InP–In contacts (0.8–1.0 eV) in the absence of hydrogen. It was reported for InP/In contacts with an evaporated indium layer that the barrier height decreases on n-type InP and increases on p-InP [8]. Our own experiments with solid state InP/In contacts where the first layer of indium was deposited electrochemically are in contradiction hereto. It was found that the current increases by a factor of 10 if an n-InP/In is exposed to an H_2 atmosphere instead of argon. But even for the p-InP/In a three times higher current is observed in hydrogen atmosphere [21]. The influence of the hydrogen on the formation and the corrosion of indium on indium phosphide under these conditions is not exactly clear. It is subject of our present investigations. However, this hydrogen influence may prove useful as some kind of switch during the deposition of the catalyst, e.g. platinum.

5. Summary

A precise Mott–Schottky analysis revealed flatband potentials and charge carrier concentrations for both types of InP in acidic solutions. The former one was almost independent on the frequency, whereas the latter showed a significant dispersion which was even stronger for n-InP. The values are graphically presented in Fig. 11.

Indium films can be prepared on InP either by cathodic decomposition in dark or by deposition of indium from $InCl_3$ containing solutions. While the first reaction forms porous films slowly, the latter reaction gives dense films immediately. The dissolution kinetics of these films was investigated, it is significantly faster for n-type InP as compared with p-type, the equilibrium potential however, is found to be -0.45 V in 1.0 M HCl containing 0.1 M $InCl_3$. The ratio between deposition and dissolution charge reveals a hydrogen evolution on p-InP in the beginning. n-Type InP, on the other hand, seems to dissolve chemically in parts in the beginning. For higher amounts of deposit, the ratio tends to unity for both types.

Hydrogen evolution is a concurrent reaction for the deposition only in the beginning and only on p-InP. During decomposition, on the other hand, it becomes a more and more important share of the total charge consumption due to the hindered material transport. No hints were found that indium does not dissolve directly into the thermodynamically stable In^{3+}. This is in contrast to other investigations [22] where In^{+} was formed instead, due to a kinetic hindrance.

Acknowledgements

The financial support of the JSPS for a postdoctoral fellowship, the Alexander von Humboldt-Stiftung and the Monbusho Grant in Aid for Scientific Research (No. 10555236) is gratefully acknowledged. We are indebted to Mr. Hiromasa Yamamoto from Japan Energy for the donation of the InP.

References

[1] K. Uosaki, H. Kita, Solar Energy Mater. 7 (1983) 421.
[2] B. Miller, J. Electroanal. Chem. 168 (1984) 91.
[3] S. Gröger, M. Handschuh, W. Lorenz, J. Electroanal. Chem. 278 (1990) 323.
[4] H. Gerischer, W. Mindt, Electrochim. Acta 13 (1968) 1329.
[5] S. Menezes, B. Miller, K.J. Bachmann, J. Vac. Sci. Technol. B 1 (1983) 48.
[6] R. Memming, Ber. Bunsenges. Phys. Chem. 91 (1987) 353.
[7] H.-M. Kühne, J. Schefold, J. Electrochem. Soc. 137 (1990) 568.
[8] J. Schefold, J. Electrochem. Soc. 139 (1992) 2862.
[9] D.E. Aspnes, A. Heller, J. Phys. Chem. 87 (1983) 4919.
[10] T. Takizawa, S. Arai, M. Nakahara, Jpn. J. Appl. Phys. 33 (1994) L643.
[11] E. Kikuno, M. Amiotti, T. Takizawa, S. Arai, Jpn. J. Appl. Phys. 34 (1995) 177.
[12] E. Hökelek, G.Y. Robinson, Appl. Phys. Lett. 40 (5) 426.
[13] A. Ismail, A.B. Brahim, J.M. Palau, L. Lassabatere, I. Lindau, Vacuum 36 (1986) 217.
[14] C. Vanleugenhaghe, M. Pourbaix, Atlas of Electrochemical Equilibria, Pergamon Press, Oxford, 1966, p. 436.
[15] L.J. Brillson, C.F. Brucker, A.D. Katnani, N.G. Stifle, R. Daniels, G. Margaritondo, Surface Sci. 132 (1983) 212.
[16] A. Ismail, J.M. Palau, L. Lassabatere, Rev. Phys. Appl. 19 (1984) 205.
[17] G. Petro, T. Kendelewicz, I.A. Babalola, I. Lindau, W.E. Spicer, J. Vac. Sci. Technol. A2 (1984) 835.
[18] A.W. Hassel, M. Aihara, M. Seo, Jap. Corr. Eng. 1999 (1999) 273.
[19] A.-M. Van Wezemael, W.H. Laflere, F. Cardon, W.P. Gomes, J. Electroanal. Chem. 87 (1978) 105.
[20] K.H. Schulte, H.J. Lewerenz, Abstract, First Gerischer Symposium (1999) 44.
[21] M. Aihara, A.W. Hassel, M. Seo, in preparation.
[22] B. Miller, R.E. Visco, J. Electrochem. Soc. 115 (1968) 251.